Conservative Scheme for the Compressible Nonhydrostatic Models with the Horizontally Explicit and Vertically Implicit Time Integration Scheme

MASAKI SATOH

Frontier Research System for Global Change/Saitama Institute of Technology, Saitama, Japan

(Manuscript received 14 March 2001, in final form 6 November 2001)

ABSTRACT

A new dynamical scheme with the conservative forms of the equations of density, momentum, and internal energy is proposed for the nonhydrostatic models. With this scheme, the conservations of the mass and the total energy are satisfied within round-off errors. In particular, methods for the integration of energy are discussed in detail, and three of the approaches are compared; one is in the form of the pressure equation, the second is the integration of internal energy with corrections on the transformation terms, and the third is use of the sum of internal energy and kinetic energy as a prognostic variable. This scheme is incorporated into a nonhydrostatic model with the horizontally explicit and vertically implicit time integration scheme for sound waves, and various numerical experiments for the dry atmosphere are performed. The numerical results show that the conservative properties are well satisfied.

1. Introduction

In recent years, the nonhydrostatic models have been used for predictions of climate change with long time integrations. Directly calculating interactions of water vapors, clouds, and radiation for several tens of days, radiative–convective equilibriums are obtained in a large domain with horizontal length from 100 to 1000 km (Held et al. 1993; Tompkins and Craig 1998b, 1999). Some research groups, on the other hand, try to extend nonhydrostatic models to cover the entire globe (Semazzi et al. 1995; Cullen et al. 1997; Qian et al. 1998; Côté et al. 1998a,b; Smolarkiewicz et al. 1999). In the near future, development of computer facilities will allow us to use high-resolution global climate models with horizontal resolution around 5–10 km. In those days, we will need to choose the nonhydrostatic equations as the dynamical framework of the climate models.

The nonhydrostatic models, or the cumulus resolving models, are nowadays developed and used by many research groups, and have shown successful simulations of mesoscale convections. These models are, however, originally intended to be used for short-range integrations of, say, a few days, so that much attention is not being paid to conservation of physical quantities. Although one needs to integrate for several tens of days to obtain a radiative–convective equilibrium (Tompkins and Craig 1998a), the conservations of mass and energy were not fully discussed in the nonhydrostatic model studies for such long-range integrations. One may think that the conservations of mass and energy are not the primary requirement for calculations of radiative–convective equilibrium or climate modeling, since there remains uncertainty derived from the artificial numerical smoothing even when the domain integral quantities are conserved. In the case that the numerical scheme does not guarantee the conservations, however, reliability of model results would be reduced at least to the range of fluctuations of the conserved quantities.

The nonhydrostatic equations have less approximations to the governing equations of the numerical models of the atmosphere, in comparison to the hydrostatic equations usually used for the large-scale models. The nonhydrostatic equations system is categorized into two groups: the incompressible system (Ogura and Phillips 1962) and the compressible system. Since the density is not a variable quantity in the incompressible system, we only consider the compressible nonhydrostatic equations in this paper. Essentially, the compressible nonhydrostatic equations are equivalent to the Euler equations in the fluid dynamics since they do not introduce any approximations to the governing equations of a fluid. As in the case of the Euler equations, the equations are formulated with the conservative forms of natural variables, that is, density, momentum, and total energy. Therefore, if these variables are discretized in the flux forms, we will obtain a conservative numerical scheme of the nonhydrostatic equations.

Such an approach according to fluid dynamics has not usually been taken in the nonhydrostatic modeling

Corresponding author address: Dr. Masaki Satoh, Saitama Institute of Technology, 1690 Fusaiji, Okabe, Oosato, Saitama 369-0293, Japan.
E-mail: satoh@sit.ac.jp

to simulate mesoscale convections. Instead of density and total energy, pressure p (or the Exner function π) and potential temperature θ (or temperature T) are usually used as prognostic variables. Historically, the choice of these variables may be due to the fact that p and T are directly measured from observations. Furthermore, The quasi-Boussinesq approximation of a deep atmosphere, which is the base of the incompressible nonhydrostatic equations, is formulated by using π and θ by Ogura and Phillips (1962). It is also an advantage of using potential temperature since θ is conserved in the Lagrangian sense in adiabatic motions and can be used as a tracer in simulations of the mesoscale convection.

The recent advance of computing resources has invoked the need for climate modeling with the nonhydrostatic equations. The importance of conservations of mass and energy is being pointed out and becoming appreciated. Doms and Schättler (1997) suggest a transition to use the equations of using density and internal energy as prognostic variables instead of pressure and enthalpy. Taylor (1984) and Gallus and Rančić (1996) have proposed the energy conserving schemes by using enthalpy or temperature as a prognostic variable. Recently, Klemp et al. (2000) have devised a conservative form of discretized equations by using density as a prognostic variable in addition to a flux form potential temperature. Xue et al. (2000) have also proposed a conservative form of discretized equations with minimum approximations to the original governing equations.

On the other hand, most of the currently used global models in the hydrostatic equations are based on the conservative forms. Arakawa and Lamb (1977) and Arakawa and Suarez (1983) developed an energy conserving scheme by considering a transformation of the kinetic energy to enthalpy based on the pressure coordinates. As an extension of this approach, there is a category of the nonhydrostatic models in which pressure in the hydrostatic balance is used as a vertical coordinate (Laprise 1992; Juang 1992; Gallus and Rančić 1996; Klemp et al. 2000). In particular, Gallus and Rančić (1996) took care of the conservation of energy in their nonhydrostatic model with the pressure coordinate. It is true that the use of the pressure coordinate in nonhydrostatic models is advantageous; it is easy to incorporate observational data to the models and the model results can be directly compared with those of the large-scale models. This does not mean, however, that the use of the pressure coordinate is the only way to the energy conserving scheme.

We think that as a horizontally resolvable scale of models becomes smaller, such as below 10 km, the geometric height z coordinate is a more appropriate choice for the vertical coordinate, since the assumption of the hydrostatic balance becomes less relevant. The height-based coordinate is used in many groups of the nonhydrostatic models, and will be an important candidate when the nonhydrostatic models are extended to the global model. In this respect, we develop a conservative numerical scheme using the height coordinate in the compressible nonhydrostatic equations. Our approach is similar to that of Taylor (1984). Although Taylor (1984) reported the vertical discretization method for the conservation of energy and entropy, we particularly concentrate on the time discretization in order to stably calculate propagation of sound waves. We also demonstrate some numerical experiments to show the usefulness of the scheme, while Taylor (1984) did not show any application of his scheme.

The structure of this paper is as follows. In section 2, we formulate a conservative scheme of the nonhydrostatic model that will be used in the following section. In particular, in section 3, the conservation of energy is discussed and alternative forms of the energy conservation are argued. In section 4, the numerical scheme is applied to some test simulations. Section 5 summarizes the results and compares them with other research.

2. Numerical scheme

a. Objectives

We summarize first the requirements of the new scheme to be developed. We are in the course of developing a global climate model in the nonhydrostatic equations to operate with a ultramassive parallel computer with distributed memories. The proposed new scheme is for the purpose of this target. First, we require conservations of variables; in particular, conservations of mass and energy are important for the climate modeling. To satisfy the conservations, we discretized the equations in the flux forms with the finite volume method. Second, the use of a massive parallel computer gives a restriction on the choice of the time integration scheme. We are only considering a horizontally two-dimensional decomposition of the domain for the parallel computation, that is, the whole horizontal computational domain consists of tiles of a rectangular area, each of which is assigned to one of computer nodes. In order to efficiently run on massive parallel computers, data communications between nodes should be smaller. Particularly, we should avoid those methods that generate global communications among many nodes, or large transfer of memory between nodes. The spectrum method and the finite element method are counted as such methods. Use of the horizontally implicit method for sound and gravity waves or the anelastic equations should be reserved since they require elliptic equations to be solved. Solving an elliptic equation on massive parallel computers usually generates large communications between nodes, although efficient numerical methods such as a multigrid method are nowadays available.

Choice of the time integration scheme greatly depends on the treatment of sound waves. We choose the

horizontally explicit and vertically implicit scheme for sound waves based on the reason described above. For a horizontally explicit scheme, one also can use the time splitting scheme (Klemp and Wilhelmson 1978; Skamarock and Klemp 1992) to accelerate the efficiency; only the terms related to sound waves are integrated by a small time step and the other slower terms such as advection terms are integrated by a large time step. The scheme shown below can incorporate the time splitting scheme, although the results with the time splitting will be omitted throughout the paper, since the conservation properties are the main concern of the present study.

We start from the Euler equations and make the least approximations to them. The Euler equations are written in the conservative forms of density, momentum, and total energy. The equation of total energy is converted to that of the internal energy, which has transformation terms with the kinetic and potential energies. We choose density ρ and internal energy e as prognostic variables. This choice is contrasted with that in the usual nonhydrostatic models where pressure p (or the Exner function π) and potential temperature θ (or temperature T) are used as prognostic variables. Here, the Exner function is defined as $\pi = (p/p_{00})^{R_d/C_p} = T/\theta$, where $p_{00} =$ 1000 hPa, R_d is the gas constant for dry air, and C_p is the specific heat at constant pressure. We will discuss these choices of the prognostic variables in terms of the ''pressure equation'' in section 2c. Furthermore, we must say that the conservation of internal energy does not mean the conservation of total energy. Even if the flux form discretization of the prognostic equation of internal energy is used, the volume integral of total energy is not conserved unless each of the transformation terms with other energies are properly discretized. We will discuss an alternative approach in section 3. In section 2e, we will modify the equations in the terrain-following coordinates for cases where topography exists.

b. The basic equations

We start from the Euler equations. The equations of density, momentum, and total energy are written as

$$\frac{\partial}{\partial t}\rho + \nabla \cdot (\rho \mathbf{v}) = 0, \tag{1}$$

$$\frac{\partial}{\partial t}(\rho v_i) + \frac{\partial}{\partial x_j}(\rho v_i v_j + p\delta_{ij} - \sigma_{ij}) = -\rho\frac{\partial \Phi}{\partial x_i}, \tag{2}$$

$$\frac{\partial}{\partial t}(\rho e^{\text{tot}}) + \nabla \cdot (\rho \mathbf{v} e^{\text{tot}} + p\mathbf{v} - v_j \sigma_{ij} + \mathbf{q}) = 0, \tag{3}$$

where $v_i (i = 1, 2, 3)$ is each a component of velocity vector $\mathbf{v} = (u, v, w)$, e^{tot} is the total energy defined by

$$e^{\text{tot}} = e + \Phi + \mathbf{v}^2/2, \tag{4}$$

where e is the internal energy and Φ is the gravitational potential. Here σ_{ij} is the stress tensor and $\mathbf{q}$ is the heat flux. We use the summation convention for the repeated indices of i or j with $x_1 = x$, $x_2 = y$, and $x_3 = z$. The Φ is a function of only z and $\partial\Phi/\partial z = g$ is the acceleration due to gravity.

Subtracting the equations of kinetic energy and potential energy from the equations of total energy (3), we have the equation of internal energy (see section 3):

$$\frac{\partial}{\partial t}(\rho e) + \nabla \cdot (\rho \mathbf{v} h) = \mathbf{v} \cdot \nabla p + Q, \tag{5}$$

where $h = e + p/\rho$ is enthalpy and

$$Q = -\nabla \cdot \mathbf{q} + \frac{\partial v_i}{\partial x_j}\sigma_{ij}, \tag{6}$$

is the diabatic term. In the case of the moist atmosphere, the latent heat release Q_m is added to the right-hand side.

As in the formulations of the usual nonhydrostatic models, we define perturbation pressure from a basic reference state that satisfies the hydrostatic balance,

$$0 = -\frac{1}{\rho_s}\nabla p_s - g. \tag{7}$$

The pressure and the density of the basic state p_s and ρ_s are determined if an appropriate temperature profile T_s is given. Using the perturbations defined by $p' = p - p_s$ and $\rho' = \rho - \rho_s$, the continuity equation (1) and the equation of motion (2) are rewritten as

$$\frac{\partial}{\partial t}\rho' + \nabla \cdot (\rho \mathbf{v}) = 0, \tag{8}$$

$$\frac{\partial}{\partial t}(\rho u) + \nabla \cdot (\rho \mathbf{v} u) = -\frac{\partial p'}{\partial x} + \frac{\partial \sigma_{xj}}{\partial x_j}, \tag{9}$$

$$\frac{\partial}{\partial t}(\rho v) + \nabla \cdot (\rho \mathbf{v} v) = -\frac{\partial p'}{\partial y} + \frac{\partial \sigma_{yj}}{\partial x_j}, \tag{10}$$

$$\frac{\partial}{\partial t}(\rho w) + \nabla \cdot (\rho \mathbf{v} w) = -\frac{\partial p'}{\partial z} - \rho' g + \frac{\partial \sigma_{zj}}{\partial x_j}. \tag{11}$$

Thus far, no approximation is introduced by the subtraction of the basic state. However, the transformation terms of energy become different forms as

$$\frac{\partial}{\partial t}(\rho e) + \nabla \cdot (\rho \mathbf{v} h) = (\mathbf{v} \cdot \nabla p' + \rho' w g) - \rho w g + Q. \tag{12}$$

The first term $(\mathbf{v} \cdot \nabla p' + \rho' w g)$ on the right is the transformation with the kinetic energy, whereas the second term $-\rho w g$ is the transformation with the potential energy.

c. The pressure equation

In the fully compressible nonhydrostatic models, the perturbation of pressure p' or the Exner function π' is

usually used as a prognostic variable instead of that of density ρ'. Normally, p' or π', T or θ, and three components of velocities are chosen for the five prognostic variables of the models. To choose p' as a prognostic variable, one need to use the pressure equation instead of the equation of density. From the thermodynamic equation, tendency of density is related to that of pressure as

$$\frac{\partial \rho}{\partial t} = \frac{1}{c_s^2}\frac{\partial p}{\partial t} - \frac{\rho}{\theta}\frac{\partial \theta}{\partial t}, \tag{13}$$

where c_s is the speed of sound, which is given, for the ideal gas, by $c_s^2 = \gamma R_d T$, where $\gamma = C_p/C_v$ and C_v is the specific heat at constant volume. From Eqs. (13) and (8), one obtains

$$\frac{1}{c_s^2}\frac{\partial p'}{\partial t} + \nabla \cdot (\rho \mathbf{v}) = \frac{\rho}{\theta}\frac{\partial \theta'}{\partial t}. \tag{14}$$

This is one of the forms of the pressure equation.

The advantage of the use of the pressure equation is that the propagation of sound waves is directly incorporated. This is typically shown by the linearized equation in an isentropic gas with no gravity. Substituting the divergence of linearized Eqs. (9)–(11) into the time derivative of Eq. (14) with $g = 0$ and $\theta' = 0$, one obtains the equation for the sound waves:

$$\frac{1}{c_s^2}\frac{\partial^2 p'}{\partial t^2} = \nabla^2 p'. \tag{15}$$

In the nonhydrostatic model, in practice, one needs to implicitly treat the terms related to the sound waves. If the pressure equation is used, p' can be implicitly calculated by solving a Helmholtz equation.

The following problems arise, however, if the pressure equation is used as a prognostic equation. First, the conservation of mass is not exactly satisfied. In fact, in the case that c_s is not constant, a volume integral of p' does not conserve when Eq. (14) is discretized in the flux form. Even when c_s is constant, it is not the total mass but the domain integral of pressure that is conserved.

The second problem, which has not been relatively noticed, is that the pressure equation is not compatible with the conservation of energy. For instance, if one integrates internal energy ρe in the flux form, it is equivalent to use pressure as a prognostic variable, since

$$\rho e = C_v \rho T = \frac{C_v}{R_d} p, \tag{16}$$

where the equation of state for the ideal gas is used. Since most of the past nonhydrostatic models use T or θ as a prognostic variable, the above problem has been avoided. For our purpose, however, the conservation of energy is required so that the use of the pressure equation should be abandoned.

In order to resolve the above two problems, we use alternative prognostic variables, ρ' and ρe, which are directly suggested from the original Euler equations. Although the pressure equation is not used, an equation for the implicit calculation of sound waves can be formulated if one notes the relation (16). That is, substituting Eq. (16) into the equation of internal energy (12) and dividing by C_v/R_d, we obtain

$$\frac{\partial}{\partial t} p + \nabla \cdot (c_s^2 \rho \mathbf{v}) = \frac{R_d}{C_v}[(\mathbf{v} \cdot \nabla p' + \rho' w g) - \rho w g + Q], \tag{17}$$

where

$$\frac{R_d}{C_v} h = \frac{R_d}{C_v} C_p T = \gamma R_d T = c_s^2 \tag{18}$$

is used for the ideal gas. Formally, Eq. (17) is analogous to the pressure equation (14). The conservation of internal energy is satisfied if Eq. (17) is discretized in the flux form even when c_s is not a constant. We have chosen a pair of the prognostic variables (ρ, ρe), which correspond to a pair of (ρ, p). In this sense, our dynamical framework is different from that with the customary used variables (p, T) or (π, θ).

In the case of no gravity, the contribution from the right-hand side of Eq. (17) vanishes in the linearized equation around the basic reference state. The convergence of the advective flux $c_s^2 \rho \mathbf{v}$ on the left-hand side, which is originally the advection of enthalpy, plays a role in the compressibility. In order to implicitly calculate propagation of sound waves, we need to treat this convergence term implicitly.

d. Time discretization

The governing equations of the nonhydrostatic model in this study are based on the flux form equations with prognostic variables being density ρ', three components of momentum ρu, ρv, ρw, and internal energy ρe. We define symbols as follows:

$$\mathbf{V} = (U, V, W) = (\rho u, \rho v, \rho w), \tag{19}$$

$$P = p', \tag{20}$$

$$R = \rho', \tag{21}$$

$$E = \rho e. \tag{22}$$

For the time integration, we use the forward scheme for U and V, and the backward scheme for R, W, and E. That is, the horizontally explicit and vertically implicit (HE–VI) scheme is used. Furthermore, we can use the time splitting scheme by partitioning terms of fast and slow motions (Klemp and Wilhelmson 1978; Skamarock and Klemp 1992).

Substituting the symbols defined above, the flux form equations (8), (9), (10), (11), and (12) become

$$\frac{\partial}{\partial t}R + \frac{\partial}{\partial x}U + \frac{\partial}{\partial y}V + \frac{\partial}{\partial z}W = 0, \tag{23}$$

$$\frac{\partial}{\partial t}U + \frac{\partial}{\partial x}P = -\nabla\cdot(\mathbf{V}u) + \frac{\partial \sigma_{xj}}{\partial x_j} \equiv G_U, \tag{24}$$

$$\frac{\partial}{\partial t}V + \frac{\partial}{\partial y}P = -\nabla\cdot(\mathbf{V}v) + \frac{\partial \sigma_{yj}}{\partial x_j} \equiv G_V, \tag{25}$$

$$\frac{\partial}{\partial t}W + \frac{\partial}{\partial z}P + Rg = -\nabla\cdot(\mathbf{V}w) + \frac{\partial \sigma_{zj}}{\partial x_j} \equiv G_W, \tag{26}$$

$$\frac{\partial}{\partial t}E + \frac{\partial}{\partial x}(Uh) + \frac{\partial}{\partial y}(Vh) + \frac{\partial}{\partial z}(Wh) - (\mathbf{v}\cdot\nabla P + Rwg) + Wg = Q. \tag{27}$$

We have placed the fast terms related to sound waves and gravity waves on the left-hand side of the equations. The choice of the implicit terms is based on the linearized equations around the reference state at rest; the terms responsible for the propagation of sound waves in the linearized equations are treated as implicit terms. Note that the buoyancy term is also treated implicitly in order to take account of the buoyancy effect on sound waves. The stability analysis of the implicit scheme of is given in the appendix. As noted when Eq. (17) is derived, the advection of enthalpy in the equation of internal energy is related to the compressibility of sound waves. This means that the advection terms in Eq. (27) should be treated implicitly.

Based on the forward–backward scheme, therefore, the time discretized forms of Eqs. (23)–(27) become

$$\delta_t R + \left(\frac{\partial U}{\partial x} + \frac{\partial V}{\partial y} + \frac{\partial W}{\partial z}\right)^{n+1} = 0, \tag{28}$$

$$\delta_t U + \frac{\partial P^n}{\partial x} = G_U^n, \tag{29}$$

$$\delta_t V + \frac{\partial P^n}{\partial y} = G_V^n, \tag{30}$$

$$\delta_t W + \frac{\partial P^{n+1}}{\partial z} + R^{n+1}g = G_W^n, \tag{31}$$

$$\delta_t E + \frac{\partial}{\partial x}(h^n U^{n+1}) + \frac{\partial}{\partial y}(h^n V^{n+1}) + \frac{\partial}{\partial z}(h^n W^{n+1}) - u^\dagger\frac{\partial P^n}{\partial x} - v^\dagger\frac{\partial P^n}{\partial x} - w^\dagger\left(\frac{\partial P^{n+1}}{\partial z} + R^{n+1}g\right) + W^{n+1}g = Q^n. \tag{32}$$

The superscripts n and $n+1$ represent the quantities of the nth and $(n+1)$th step in the time integration and we express

$$\delta_t A = (A^{t+\Delta t} - A^t)/\Delta t = (A^{n+1} - A^n)/\Delta t. \tag{33}$$

In Eq. (32), we have introduced $u^\dagger$, $v^\dagger$, and $w^\dagger$, whose discretization should be determined so as to keep the consistency of the transformation between the internal energy and the kinetic energy. We will argue about the transformations of energy and the possible forms of $u^\dagger$, $v^\dagger$, and $w^\dagger$ in section 3. Here, we proceed using a practical approach.

Equations (28)–(32) are integrated via two steps. First, the $(n+1)$th step values of U, V are calculated from Eqs. (29) and (30), respectively. The equation of the internal energy (32) is transformed to the equation of P using Eq. (16). A set of Eqs. (28), (31), and (32), therefore, consists of the implicit equations for the three variables, R^{n+1}, W^{n+1}, and P^{n+1}. It is troublesome to solve for the $(n+1)$th step variables, however, if $u^\dagger$, $v^\dagger$, and $w^\dagger$ contains either R^{n+1}, W^{n+1}, or P^{n+1}. To avoid the nonlinearity of the $(n+1)$th step variables, we choose

$$u^\dagger = \frac{U^n + U^{n+1}}{2(\rho_s + R^n)}, \qquad v^\dagger = \frac{V^n + V^{n+1}}{2(\rho_s + R^n)}. \tag{34}$$

Under the condition that the change in density is small, the transformation with the kinetic energy of the horizontal winds is consistent with the equation of momentum as will be discussed in section 3. We also replace the term in Eq. (32) as

$$w^\dagger\left(\frac{\partial P^{n+1}}{\partial z} + R^{n+1}g\right) \rightarrow \frac{W^{n+1}}{\rho_s + R^n}\left(\frac{\partial P^n}{\partial z} + R_n g\right). \tag{35}$$

Although the left-hand side contains nonlinear terms of $(n+1)$th, step variables to keep the conservation (section 3), this replacement makes it linear and thus the implicit calculation can be easily performed. This term is an effect of stratification on sound/gravity waves. The use of the right-hand side means that the nth step stratification is used as a basic state and does not affect linear propagation of sound/gravity waves. On the other hand, the transformation of energy becomes incomplete with this approximation. We will make a correction when the integration of E is performed [see Eq. (47) below]. Using Eq. (16), the equation of internal energy (32) is transformed to

$$\delta_t P + \frac{\partial}{\partial z}(c_s^2 W^{n+1}) + \frac{R_d}{C_v}W^{n+1}\tilde{g} = \frac{R_d}{C_v}G_E^n, \tag{36}$$

where

$$c_s^2 \equiv \frac{R_d}{C_v} h^n = \gamma R_d T^n, \tag{37}$$

$$\tilde{g} \equiv g - \frac{1}{\rho_s + R^n}\left(\frac{\partial P^n}{\partial z} + R^n g\right), \tag{38}$$

$$G_E^n \equiv -\frac{\partial}{\partial x}(U^{n+1}h^n) - \frac{\partial}{\partial y}(V^{n+1}h^n) + u^\dagger \frac{\partial P^n}{\partial x} + v^\dagger \frac{\partial P^n}{\partial y} + Q^n. \tag{39}$$

In the case of the hydrostatic balance, $\tilde{g}$ agrees with the acceleration due to gravity g.

We are in a position of describing how the equations are integrated. First, from Eqs. (29) and (30),

$$U^{n+1} = U^n + \Delta t\left(-\frac{\partial P^n}{\partial x} + G_U^n\right), \tag{40}$$

$$V^{n+1} = V^n + \Delta t\left(-\frac{\partial P^n}{\partial y} + G_V^n\right). \tag{41}$$

The remaining variables R^{n+1}, W^{n+1}, P^{n+1} are solved by the implicit calculation of the three equations (28), (31), and (36). They are formally solved for the $(n + 1)$th step:

$$R^{n+1} = R^n + \Delta t\left(-\frac{\partial W^{n+1}}{\partial z} + G_R^n\right), \tag{42}$$

$$W^{n+1} = W^n + \Delta t\left(-\frac{\partial P^{n+1}}{\partial z} - R^{n+1}g + G_W^n\right), \tag{43}$$

$$P^{n+1} = P^n + \Delta t\left[-\frac{\partial}{\partial z}(c_s^2 W^{n+1}) - \frac{R_d}{C_v} W^{n+1}\tilde{g} + \frac{R_d}{C_v} G_E^n\right], \tag{44}$$

where

$$G_R^n = -\left(\frac{\partial U}{\partial x} + \frac{\partial V}{\partial y}\right)^{n+1}. \tag{45}$$

Substituting R^{n+1} and P^{n+1} of Eqs. (42) and (44) into Eq. (43), we obtain a Helmholtz equation for W^{n+1}:

$$-\frac{\partial^2}{\partial z^2}(\Delta t^2 c_s^2 W^{n+1}) - \left[\frac{\partial}{\partial z}\left(\Delta t^2 \frac{R_d}{C_v}\tilde{g}W^{n+1}\right) + \Delta t^2 g \frac{\partial W^{n+1}}{\partial z}\right] + W^{n+1} = W^n + \Delta t G_W^n - \Delta t \frac{\partial}{\partial z}\left(P^n + \Delta t \frac{R_d}{C_v} G_E^n\right) - \Delta t g(R^n + \Delta t G_R^n). \tag{46}$$

If we use the first-order discretization in the vertical gradient, this equation is discretized as a form of a tri-diagonal matrix multiplied by the vector W^{n+1}. This type of equation is easily solved.

The density R^{n+1} is integrated with a conservative flux form by substituting W^{n+1} into Eq. (42). Similarly, P^{n+1} can be integrated by using Eq. (44). The replacement of Eq. (35), however, introduced inconsistency in the transformation of energy. Then, we recover Eq. (32) instead of (44) to integrate E, that is,

$$E^{n+1} = E^n + \Delta t\left[-\frac{\partial}{\partial x}(h^n U^{n+1}) - \frac{\partial}{\partial y}(h^n V^{n+1}) - \frac{\partial}{\partial z}(h^n W^{n+1}) + \overline{u}\frac{\partial P^n}{\partial x} + \overline{v}\frac{\partial P^n}{\partial x} + \overline{w}\left(\frac{\partial P^{n+1}}{\partial z} + R^{n+1}g\right) - W^{n+1}g + Q^n\right], \tag{47}$$

where $\overline{A} = (A^n + A^{n+1})/2$. It is clear that E^{n+1} obtained by (47) and P^{n+1} obtained by (44) do not satisfy the relation (16). Precisely, one needs to iterate for E^{n+1} and P^{n+1}; number of iterations should be determined by the relative importance between the accuracy and the computation time. For our purpose, however, no iteration is needed as long as the integration is stable, since it is thought that the accuracy of sound waves is unimportant.

In the above formula, we derived the Helmholtz equation for W^{n+1}. The other choice of the equation for R^{n+1} or P^{n+1} may be considered. One of the advantages of solving for W is that the top and the bottom boundary conditions are easily incorporated; in the case when the kinematic condition is applied at the boundaries, the boundary values of W^{n+1} are directly given. In addition, round-off errors will be smaller if R^{n+1} and E^{n+1} are directly integrated using the flux form equations. In particular, by using the energy equation (47), we can make a correction for the errors introduced when Eq. (36) is derived. Furthermore, if the specific heat depends on temperature or humidity, Eq. (36) is only an approximation. Equation (47) satisfies the conservation since the advection term is written in the flux form.

e. Terrain-following coordinate

The conservation form of the equations is extended to the terrain-following coordinate when the surface has a topography. We summarize here the flux form equations in the terrain following coordinate. We assume that a new vertical coordinate ξ is steady and monotonic in the vertical direction. A simplest example of ξ is

$$\xi = \frac{z_T(z - z_s)}{z_T - z_s}, \tag{48}$$

where z_T is the top of the model domain and z_s is the height of the surface. This coordinate is used for the simulation of topographic waves in section 4d.

The metrics are defined as

$$G^{1/2} \equiv \left(\frac{\partial z}{\partial \xi}\right)_{x,y} = \frac{1}{\left(\frac{\partial \xi}{\partial z}\right)_{x,y}}, \qquad G^{13} \equiv \left(\frac{\partial \xi}{\partial x}\right)_z,$$

$$G^{23} \equiv \left(\frac{\partial \xi}{\partial y}\right)_z, \tag{49}$$

$$J_x \equiv \left(\frac{\partial z}{\partial x}\right)_\xi = -G^{1/2}G^{13},$$

$$J_y \equiv \left(\frac{\partial z}{\partial y}\right)_\xi = -G^{1/2}G^{23}. \tag{50}$$

Mass element within a vertical length δz is $\delta m = \rho \delta z$. Denoting the corresponding length in the ξ coordinate by $\delta\xi$, we have

$$\delta m = \rho \delta z = \rho \frac{\partial z}{\partial \xi}\delta\xi = G^{1/2}\rho d\xi. \tag{51}$$

Hence, the prognostic variable of the equation of ϕ is transformed to $G^{1/2}\rho\phi$ in the flux form equation. We also have the transformation of the derivatives:

$$G^{1/2}\left(\frac{\partial \phi}{\partial x}\right)_z = \frac{\partial}{\partial x}(G^{1/2}\phi)|_\xi - \frac{\partial}{\partial \xi}(J_x\phi)|_{x,y}$$
$$= \frac{\partial}{\partial x}(G^{1/2}\phi)|_\xi + \frac{\partial}{\partial \xi}(G^{1/2}G^{13}\phi)|_{x,y}, \tag{52}$$

$$G^{1/2}\left(\frac{\partial \phi}{\partial y}\right)_z = \frac{\partial}{\partial y}(G^{1/2}\phi)|_\xi - \frac{\partial}{\partial \xi}(J_y\phi)|_{x,y}$$
$$= \frac{\partial}{\partial y}(G^{1/2}\phi)|_\xi + \frac{\partial}{\partial \xi}(G^{1/2}G^{23}\phi)|_{x,y}, \tag{53}$$

$$G^{1/2}\left(\frac{\partial \phi}{\partial z}\right)_{x,y} = \left(\frac{\partial \phi}{\partial \xi}\right)_{x,y}. \tag{54}$$

Thus, the divergence of a flux $\mathbf{F} = (F_x, F_y, F_z)$ is expressed as

$$G^{1/2}\nabla\cdot\mathbf{F} = G^{1/2}\frac{\partial F_x}{\partial x} + G^{1/2}\frac{\partial F_y}{\partial y} + G^{1/2}\frac{\partial F_z}{\partial z}$$
$$= \left(\frac{\partial (G^{1/2}F_x)}{\partial x}\right)_\xi + \left(\frac{\partial (G^{1/2}F_y)}{\partial y}\right) + \frac{\partial}{\partial \xi}F_z^*, \tag{55}$$

where

$$F_z^* = F_z - J_xF_x - J_yF_y$$
$$= F_z + G^{1/2}G^{13}F_x + G^{1/2}G^{23}F_y. \tag{56}$$

The vertical velocity in the ξ coordinate is

$$\dot{\xi} \equiv \frac{d\xi}{dt} = G^{13}u + G^{23}v + \frac{1}{G^{1/2}}w = \frac{1}{G^{1/2}}w^*, \tag{57}$$

where

$$w^* = w - J_xu - J_yv$$
$$= w + G^{1/2}G^{13}u + G^{1/2}G^{23}v. \tag{58}$$

Therefore, multiplying $G^{1/2}$ to the equation,

$$\frac{\partial}{\partial t}(\rho\phi) + \frac{\partial}{\partial x}(\rho\phi u + F_x) + \frac{\partial}{\partial y}(\rho\phi v + F_y)$$
$$+ \frac{\partial}{\partial z}(\rho\phi w + F_z) = S, \tag{59}$$

we have the flux form equation in the (x, y, ξ) coordinates as

$$\frac{\partial}{\partial t}(G^{1/2}\rho\phi) + \frac{\partial}{\partial x}(G^{1/2}\rho\phi u + G^{1/2}F_x)$$
$$+ \frac{\partial}{\partial y}(G^{1/2}\rho\phi v + G^{1/2}F_y) + \frac{\partial}{\partial \xi}(\rho\phi w^* + F_z^*)$$
$$= G^{1/2}S. \tag{60}$$

By transforming Eqs. (23)–(27) using this formula, we obtain a set of the equations in the terrain following coordinate.

3. Energy budget

a. Transformation of energy

In section 2d, we described the time discretization of the model equations. We have pointed out that each of the transformation terms of energy should be consistently discretized to satisfy the conservation of energy, and have presented one possible approach. In this section, we consider how the conservation of energy is satisfied in the numerical scheme and argue about alternative forms of the equation of energy.

The total energy is defined as the sum of kinetic energy, potential energy, and internal energy as Eq. (4). The change in each energy is written as

$$\frac{\partial}{\partial t}\left(\rho\frac{\mathbf{v}^2}{2}\right) + \nabla\cdot\left(\rho\mathbf{v}\frac{\mathbf{v}^2}{2}\right) = -\mathbf{v}\cdot\nabla p' - \rho' wg$$
$$+ v_i\frac{\partial \sigma_{ij}}{\partial x_j}, \tag{61}$$

$$\frac{\partial}{\partial t}(\rho\Phi) + \nabla\cdot(\rho\Phi\mathbf{v}) = \rho wg, \tag{62}$$

$$\frac{\partial}{\partial t}(\rho e) + \nabla\cdot(\rho\mathbf{v}h) = (\mathbf{v}\cdot\nabla p' + \rho' wg)$$
$$- \rho wg + Q. \tag{63}$$

The sum of Eqs. (61), (62), and (63) gives the conservation of total energy Eq. (3). Let us denote the trans-

formation term from the potential energy to the internal energy by $C_{\rm PI}$, and that from the kinetic energy to the internal energy by $C_{\rm KI}$:

$$C_{\rm PI} = -\rho wg, \tag{64}$$

$$C_{\rm KI} = \mathbf{v}\cdot\nabla p' + \rho' wg. \tag{65}$$

Note that the contribution of the stress tensor is not considered here. To satisfy the conservation of total energy, we need to consistently discretize these transformation terms.

The form of $C_{\rm PI}$ depends on the discretization of the equation of density. We have chosen Eq. (28) for the equation of density. In this case, the corresponding change in the potential energy is written as

$$\begin{aligned}\delta_t(\rho\Phi) &+ \frac{\partial}{\partial x}(U^{n+1}\Phi) + \frac{\partial}{\partial y}(V^{n+1}\Phi) + \frac{\partial}{\partial z}(W^{n+1}\Phi)\\ &= \Phi\left(\delta_t\rho + \frac{\partial}{\partial x}U^{n+1} + \frac{\partial}{\partial y}V^{n+1} + \frac{\partial}{\partial z}W^{n+1}\right) + W^{n+1}g\\ &= W^{n+1}g.\end{aligned} \tag{66}$$

Thus, the transformation from the potential energy to the internal energy should be expressed as

$$C_{\rm PI} = -W^{n+1}g. \tag{67}$$

As for the transformation term $C_{\rm KI}$, the exact conservation is not satisfied since the discretization is not complete as shown below. When each of the velocity components are chosen as the prognostic variables, the change in the kinetic energy is derived from the discretized equations of momentum. Actually, the equation of kinetic energy (61) is given by the inner product of the equations of momentum (2) and the velocity vector using the equation of density (1). By using a formula,

$$\overline{A}\delta_t B + \overline{B}\delta_t A = \delta_t(AB), \tag{68}$$

we have the discretized relation for the change in kinetic energy:

$$\begin{aligned}\overline{u}\delta_t U + \overline{v}\delta_t V + \overline{w}\delta_t W - (\overline{\mathbf{v}^2}/2)\delta_t R\\ = \delta_t K - (\overline{\mathbf{V}} - \overline{\rho}\,\overline{\mathbf{v}})\cdot\delta_t\mathbf{v},\end{aligned} \tag{69}$$

where the kinetic energy is defined by

$$\begin{aligned}K^n &= \rho^n\frac{(u^n)^2 + (v^n)^2 + (w^n)^2}{2}\\ &= \frac{1}{\rho^n}\frac{(U^n)^2 + (V^n)^2 + (W^n)^2}{2}.\end{aligned} \tag{70}$$

The second term on the right-hand side of Eq. (69) is a discretization error. From Eqs. (28), (29), (30), and (31), the discretized equation of kinetic energy is given by

$$\begin{aligned}\delta_t K = &-\overline{u}\frac{\partial P^n}{\partial x} - \overline{v}\frac{\partial P^n}{\partial y} - \overline{w}\left(\frac{\partial P^{n+1}}{\partial z} + R^{n+1}g\right)\\ &+ \overline{u}G_U^n + \overline{v}G_V^n + \overline{w}G_W^n\\ &+ \frac{\overline{\mathbf{v}^2}}{2}\left(\frac{\partial U}{\partial x} + \frac{\partial V}{\partial y} + \frac{\partial W}{\partial z}\right)^{n+1}\\ &+ (\overline{\mathbf{V}} - \overline{\rho}\,\overline{\mathbf{v}})\cdot\delta_t\mathbf{v}.\end{aligned} \tag{71}$$

The corresponding discretized form of the transformation term is

$$C_{\rm KI} = \overline{u}\frac{\partial P^n}{\partial x} + \overline{v}\frac{\partial P^n}{\partial y} + \overline{w}\left(\frac{\partial P^{n+1}}{\partial z} + R^{n+1}g\right), \tag{72}$$

which is introduced in Eq. (47).

It is clear from Eq. (71) that the conservation of kinetic energy is not exactly satisfied, since $\overline{\rho}$ is time dependent and the last term on the right-hand side of Eq. (71) remains as a discretization error. The other difficulty comes from the advection of the momentum. The advection of kinetic energy in the third line on the right-hand side of Eq. (71) is not be rewritten as a flux form, since the velocities of the nth and $(n+1)$th step values are contaminated. In general, when the equation of kinetic energy is constructed from the equations of momentum, the advection of kinetic energy is not expressed in the flux form; this will be another source of the change in total energy. As for the incompressible fluid, for instance, Morinishi et al. (1998) have proposed a tactful discretization of the advection of momentum so that the advection of kinetic energy is written in the flux form. It is widely believed, however, that the contribution of the advection of kinetic energy is small in the budget of total energy. In the numerical scheme presented in section 2d, therefore, the total energy is approximately conserved in the case that the contribution of density change and the advection of kinetic energy are negligible.

b. Integration of the sum of internal energy and kinetic energy

As a totally different approach to the exact conservation of total energy, one could choose the sum of internal energy and kinetic energy as a prognostic variable. We have implicitly solved for the variables R, W, and P from Eqs. (42), (43), and (44) for the vertical propagation of sound waves. In general, the internal energy E obtained by the following method does not satisfy the relation (36) with P. Nevertheless, as in the same thought of using Eq. (47) for the prediction of E, the following method may be used as an iterative process, if the difference of E obtained by the two methods is small.

From Eqs. (61) and (63), the change in the sum of internal energy and kinetic energy is written as

$$\frac{\partial}{\partial t}\left[\rho\left(e + \frac{\mathbf{v}^2}{2}\right)\right] + \nabla\cdot\left[\rho\mathbf{v}\left(h + \frac{\mathbf{v}^2}{2}\right)\right] = -\rho wg - \nabla\cdot\mathbf{q} + \frac{\partial}{\partial x_j}(v_i\sigma_{ij}), \quad (73)$$

where Eq. (6) is used. The discretized form may be given as

$$\delta_t(E + K) = -\nabla\cdot\left[\mathbf{V}^{n+1}\left(h + \frac{\mathbf{v}^2}{2}\right)^n\right] - W^{n+1}g - \nabla\cdot\mathbf{q}^n + \frac{\partial}{\partial x_j}(v_i\sigma_{ij})^n. \quad (74)$$

In the advection term, the $(n + 1)$th step velocity $\mathbf{V}^{n+1}$ is used; it is required from the stability of the propagation of sound waves. The transformation term with the potential energy is expressed by using Eq. (67). Since K^{n+1} is already given from the $(n + 1)$th step values of U, V, W, and R, E^{n+1} is given by subtracting K^{n+1} from $(E + K)^{n+1}$, which is integrated by the above equation.

c. Integration of entropy

In the last part of this section, we comment on the conservation of entropy in comparison to the conservation of energy. In many nonhydrostatic models, the potential temperature is used as a prognostic variable. For instance, Ooyama (1990) argues that the choice of entropy as a prognostic variable is preferable. Klemp et al. (2000) follows the argument of Ooyama in their flux form equations. The formulation of Ooyama (1990), however, is based on the adiabatic process, so that his form is insufficient for the cases that the energy input is important as in the climate modeling. The change in potential temperature is written as

$$\frac{\partial}{\partial t}(\rho\theta) + \nabla\cdot(\rho\mathbf{v}\theta) = \frac{\theta}{C_pT}Q. \quad (75)$$

The diabatic heating Q is given by Eq. (6). For the climate modeling, the convergence of the heat flux $-\nabla\cdot\mathbf{q}$ has an important contribution. If one uses the equation of the internal energy (5), the domain integral of the source term $\int Q\,dV$ leaves only the boundary values of the heat flux, for example, the sensible heat flux from the surface and the radiative fluxes at the top and the bottom boundaries of the atmosphere. On the other hand, if one uses the equation of potential temperature based on a discretized form of Eq. (75), the change in the domain integral of total energy is generally different from energy input from the boundaries, since temperature is diagnostically calculated form potential temperature. This will cause an error of the energy budget. As for the discretization of general circulation models, for instance, the conservation of energy is formulated based on the change in enthalpy as described by Arakawa and Lamb (1977) and Arakawa and Suarez (1983). They use an additional requirement that the domain integral of potential temperature remains constant under the adiabatic condition to eliminate an arbitrary choice of the vertical discretization. We also follow the Arakawa's concept that the first principle is the conservation of energy, that is, internal energy or enthalpy, but not the conservation of entropy.

The similar approach is adopted by Taylor (1984) who followed Arakawa and Lamb (1977) and devised the vertical discretization scheme using the height z as the vertical coordinate. Taylor uses the equation of enthalpy as a prognostic equation, and guarantees the conservations of potential temperature and entropy by appropriate vertical interpolations of thermodynamic variables. If we use such a vertical discretization as Taylor's, potential temperature and entropy will be also conserved even when the internal energy is chosen as a prognostic variable.

4. Model and results

a. Model

We show some results for simple simulations using the numerical scheme described in sections 2 and 3. We have proposed three methods of the energy integration. The first method is based on Eq. (44), from which E^{n+1} is given by multiplication of C_v/R_d to P^{n+1}: this is referred to as the ''noncorrection'' method. The second is based on Eq. (47) where the correction is made to the transformation terms of energies: this method is referred to as the ''correction'' method. In the third method, the conservation of the total energy is guaranteed based on Eq. (74): this will be called the ''conservative'' method. The results of using these methods are compared in some of the following experiments.

The model is developed in the three-dimensional Cartesian coordinate, but only the results for the two-dimensional calculations are shown here. The definition points of the variables are based on the Arakawa C grid; R, E, and P are defined at the same points, and U, V, and W are defined at the staggered points shifted half point in the x, y, and z directions, respectively. The Lorenz grid is used in the vertical direction. Rigid walls are placed at the bottom and the top of boundaries and free slip and insulating conditions are used at the boundaries. Periodicity is assumed at the lateral boundaries. The time integration of sound waves is based on the forward–backward scheme; the horizontally explicit and vertically implicit scheme as described in section 2d. The model is constructed following the time splitting method (Klemp and Wilhelmson 1978; Skamarock and Klemp 1992), but we simply set the small time step equal to the large time step. The large time step is integrated with the leapfrog scheme with the time filter to suppress the computational mode. We denote the time step of the leapfrog scheme as $2\Delta t$, where $2\Delta t$ is equal

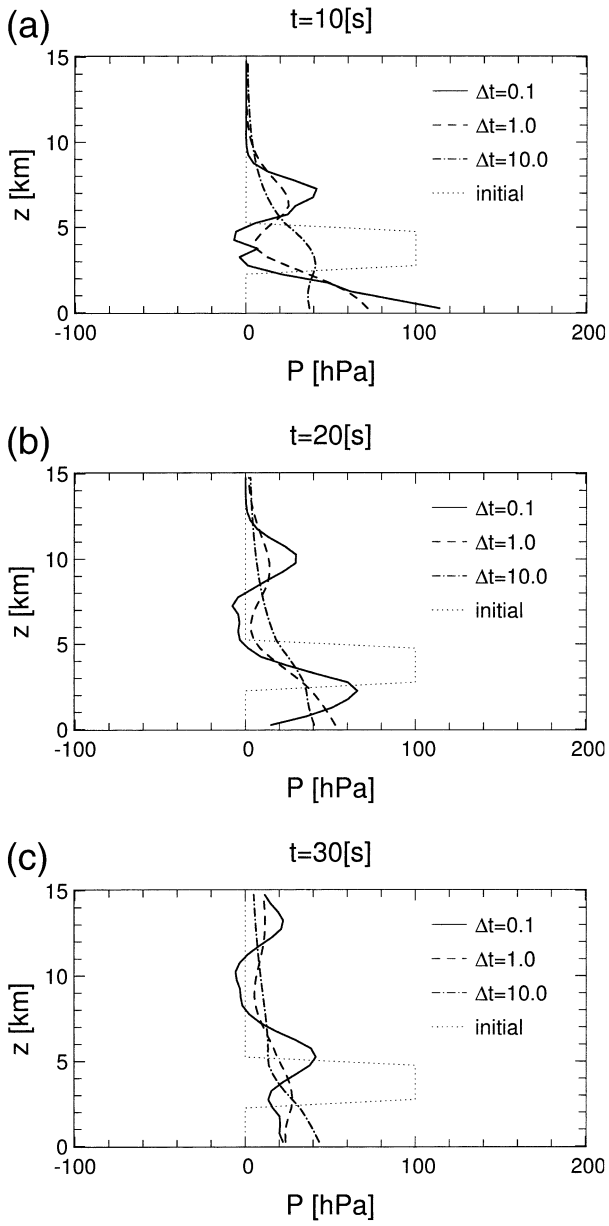

FIG. 1. Vertical profiles of perturbations of pressure p' for the experiments of the vertical propagation of sound waves at (a) t = 10, (b) 20, and (c) 30 s. The initial state is shown by the dotted curve and the experiments with Δt = 0.1, 1.0, and 10.0 s are shown by the solid, dashed, and dashed–dotted curves, respectively.

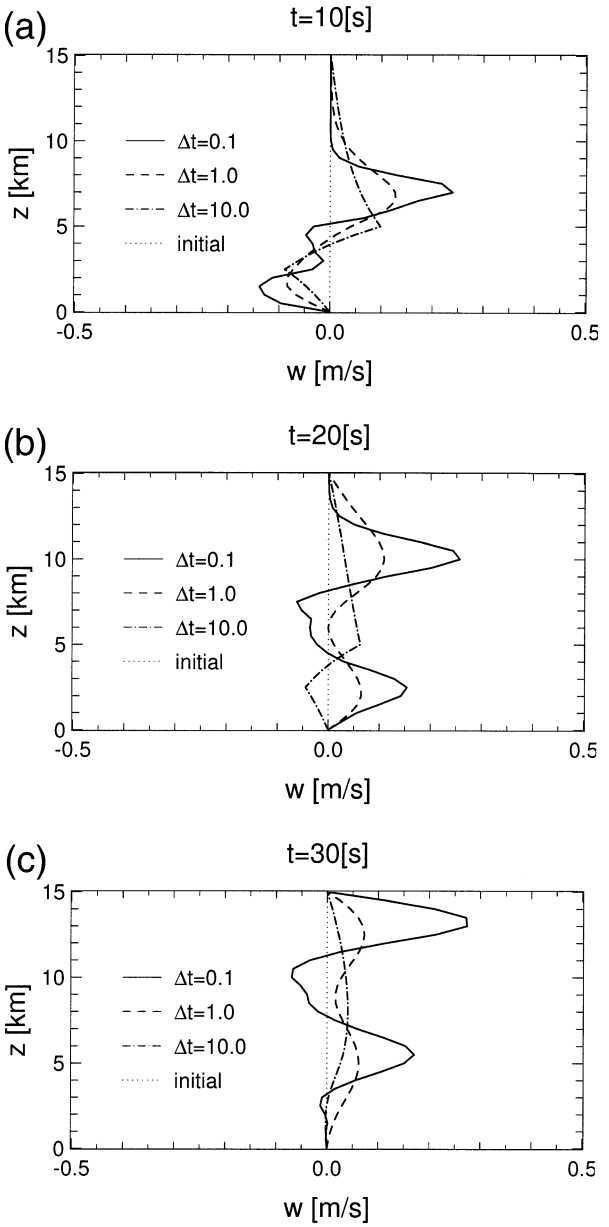

FIG. 2. The same as in Fig. 1 but for the vertical velocity w.

to the time step of the forward–backward scheme of sound waves. We use a simple second-order centered-in-space scheme for the advections.

b. One-dimensional vertical propagation of sound waves

First, we calculate vertically propagating sound waves to see the stability of the scheme. A perturbation of pressure is given in a layer at the initial state under a horizontally uniform condition. The initial state is uniform temperature 250 K at rest in the hydrostatic balance except for the perturbation of pressure p' = 100 hPa between the heights 2.5 and 5 km. The top of the atmosphere is z_T = 15 km, and the layer difference is uniform with Δz = 500 m. No numerical smoothing such as numerical diffusion, Rayleigh damping, or the time filter is introduced in this case. Note that, however, the fully implicit scheme has a damping characteristic (see the appendix).

First, we use the correction method for the energy integration. Figures 1 and 2 show the vertical distributions of pressure and vertical velocity, respectively,

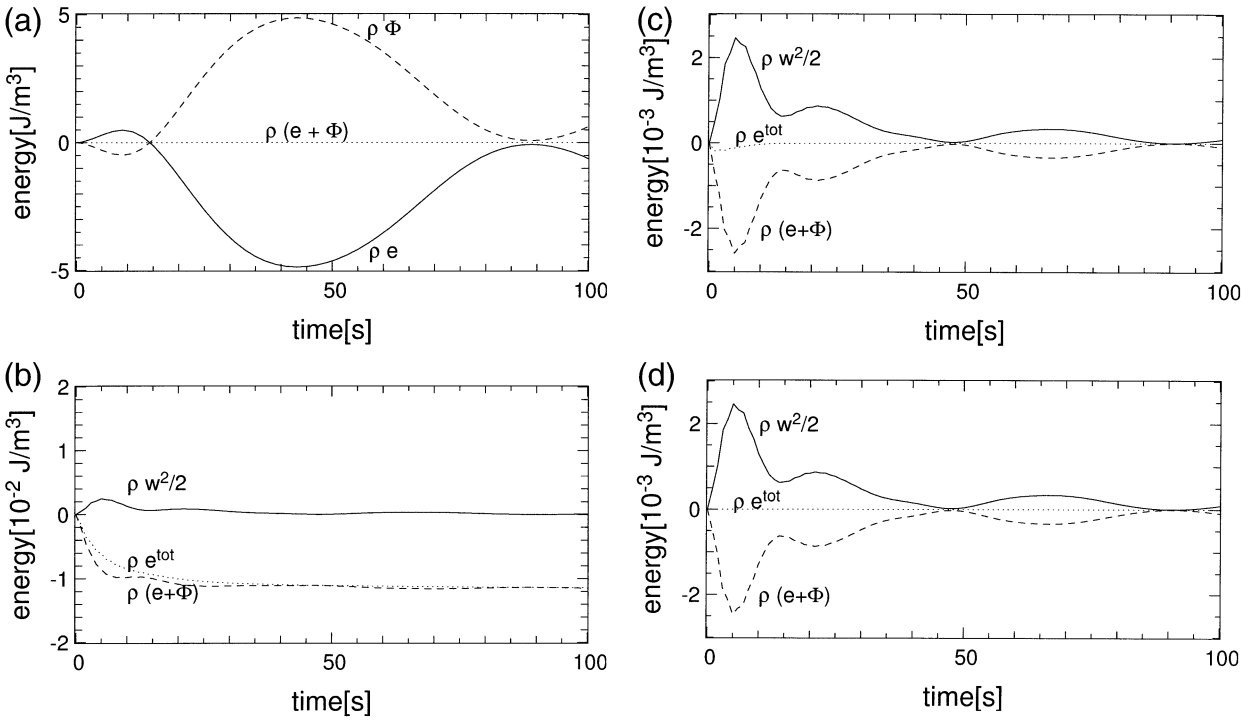

FIG. 3. Time sequences of energies for the experiments of the vertical propagation of sound waves with $\Delta t = 1$ s. (a) Internal energy ρe (solid), potential energy $\rho\Phi$ (dashed), and available potential energy $\rho(e + \Phi)$ (dotted). (b), (c), (d) Kinetic energy $\rho w^2/2$ (solid), available potential energy $\rho(e + \Phi)$ (dashed), and total energy ρe^{tot} (dotted). (a), (b) The noncorrection method, (c) the correction method, and (d) the conservative method (see text). Values of the energies are the differences from the initial values and averaged for a unit volume: the dimension is J m^{-3}.

at $t = 10$, 20, and 30 s. We compare the profiles with the time step $\Delta t = 0.1$, 1, and 10 s. It can be confirmed that the case with $\Delta t = 10$ s, which is larger than the Courant–Friedrichs–Lewy (CFL) criterion for the sound wave, is stably integrated. Since the fully implicit scheme is used for the vertical propagation of sound waves, the amplitude of pressure perturbation rapidly decreases as Δt becomes larger (see the appendix). The characteristics of these figures are almost the same for the three methods of the energy integration. The difference between the methods is shown if the energy budget is examined.

The conservation properties are investigated for the case $\Delta t = 1$ s. The total mass should be constant as long as no coding error is introduced. In the present calculation, the change in the mean density is within 10^{-15} kg m^{-3} until $t = 1000$ s, which comes from the numerical round-off errors. Figure 3 shows time sequences of energies until $t = 100$ s: internal energy ρe, potential energy $\rho\Phi$, and kinetic energy $\rho w^2/2$. Here, we define the total energy e^{tot} and the available potential energy e^{avail}:

$$e^{\text{avail}} = e + \Phi, \tag{76}$$

$$e^{\text{tot}} = e + \Phi + \mathbf{v}^2/2 = e^{\text{avail}} + \mathbf{v}^2/2. \tag{77}$$

We use the name ''available energy'' since we will consider only the time change in the volume integral of e^{avail}; the change in e^{avail} must be canceled out with the change in kinetic energy in the analytic form. In these figures, the differences of the volume-averaged values from those initial values are shown. Figure 3a shows that the change in ρe is almost balanced by the change in $\rho\Phi$. The change in the potential energy is due to the change in the height of the center of gravity. The small difference between ρe and $\rho\Phi$ is reflected in the available potential energy ρe^{avail}, which is transformed with the kinetic energy $\rho w^2/2$. In this set up, the total energy is analytically conserved since there is no energy input. The conservation of total energy in the numerical scheme is not guaranteed, however, unless the transformation between kinetic energy and available potential energy is taken care of. The changes in the total energy for the three methods of the energy integration are compared in Figs. 3b,c, and 3d. In the case of the noncorrection method, in which no special care is taken for the transformation, the change in the kinetic energy is very different from the change in the available potential energy (Fig. 3b). In the case of the correction method and the conservative method, on the other hand, the change in the kinetic energy is almost canceled out by the change in the available potential energy and the total energy is almost conserved (Figs. 3c and 3d), although the change in the total energy of the correction method is slightly different from zero. This result im-

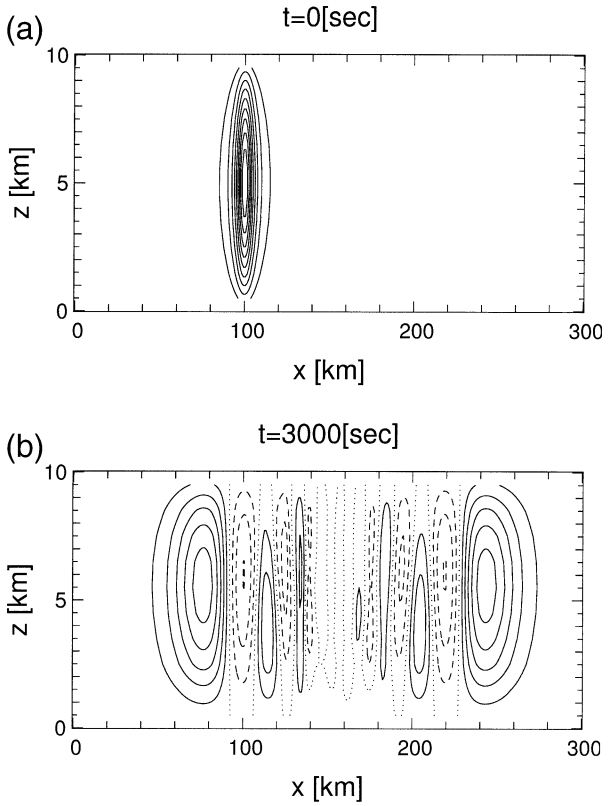

FIG. 4. Distributions of perturbations of potential temperature for the experiment of the horizontal propagation of gravity waves at (a) the initial state and (b) $t = 3000$ s. The contour intervals are (a) 10^{-3} K and (b) 0.5×10^{-3} K. The solid curves are positive, the dashed curves are negative, and the dotted curves are zero.

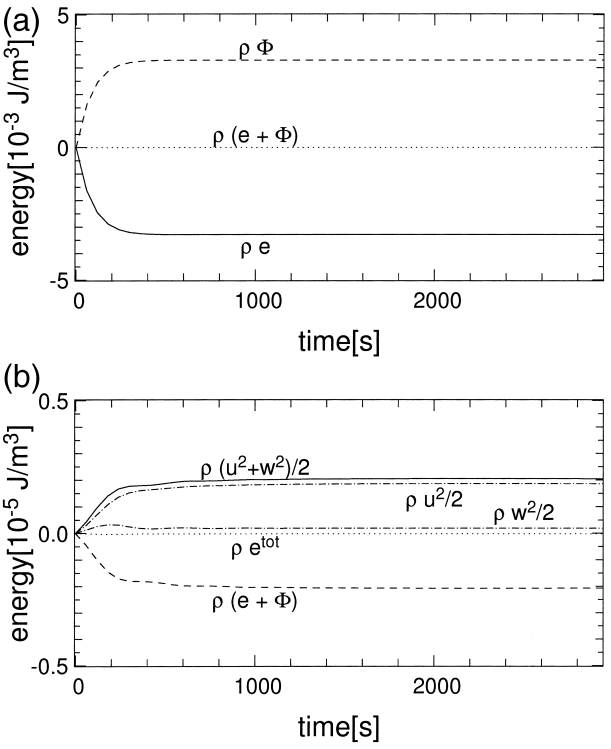

FIG. 5. The same as Figs. 3a and 3b but for the experiment of the horizontal propagation of gravity waves. In (b), the total kinetic energy $\rho(u^2 + w^2)/2$ (solid), $\rho u^2/2$ and $\rho w^2/2$ (dashed–dotted) are added.

plies that the noncorrection method is inappropriate in terms of the conservation of the total energy. Since the nonlinear advection terms are not important in this experiment, the results of the correction method and the conservative method are almost similar.

c. Horizontal propagation of gravity waves

Second, we calculate horizontal propagation of gravity waves by giving potential temperature perturbations initially. The purpose of this experiment is to examine whether the propagation of gravity waves is properly calculated in our scheme in which the buoyancy term is implicitly treated. The experimental condition is the same as that given by Skamarock and Klemp (1994). The top of atmosphere is $z_T = 10$ km, and the horizontal domain size is 300 km in the x direction. The grid interval is $\Delta x = \Delta z = 1$ km and the time step is $\Delta t = 1$ s. The coefficient of the time filter is 0.05. We do not introduce divergence damping or any other numerical smoothing. The correction method is used for the energy integration. The initial thermal state has a constant Brunt–Väisälä frequency with $N^2 = 10^{-4}\ \mathrm{s}^{-2}$. The temperature at the bottom of the atmosphere is 300 K. The initial profile of potential temperature perturbation is given by

$$\theta' = \Delta\theta_0 \frac{\sin(\pi z/z_T)}{1 + (x - x_m)^2/x_r^2}, \tag{78}$$

where $\Delta\theta_0 = 0.01$ K, $x_m = 100$ km, and $x_r = 5$ km. The uniform horizontal wind 20 m s^{-1} is given. Note that this experiment is different from that given by Skamarock and Klemp (1994) where vertical variation of density is not considered, whereas we are using the ideal gas. The similar experiment with the ideal gas is shown by Bonaventura (2000).

Figure 4 shows the distributions of potential temperature at the initial state and $t = 3000$ s. Although a slight asymmetry emerges in the vertical direction, the horizontal propagation of the gravity waves almost agrees with the analytic solution shown by Skamarock and Klemp (1994).

Figure 5 shows time sequences of the volume-averaged values of energies. The differences from the initial values are shown. Similar to Fig. 3, the conservation of total energy is well satisfied. In particular, as shown by Fig. 5b, the transformation between the kinetic energy and the available energy is appropriately calculated. The change in mass is negligibly small though the mass is increasing due to the round-off error: the change in the mean density is below 10^{-13} kg m^{-3}.

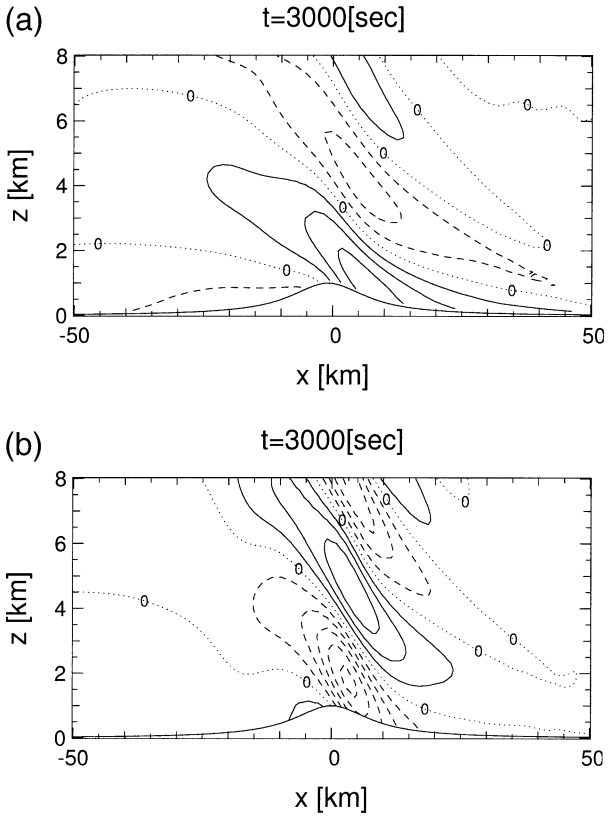

FIG. 6. Distributions of perturbations of (a) horizontal velocity and (b) vertical velocity for the experiment of the finite amplitude topographic waves at $t = 3000$ s. The contour intervals are (a) 6 and (b) 0.6 m s^{-1}. The solid curves are positive, the dashed curves are negative, and the dotted curves are zero.

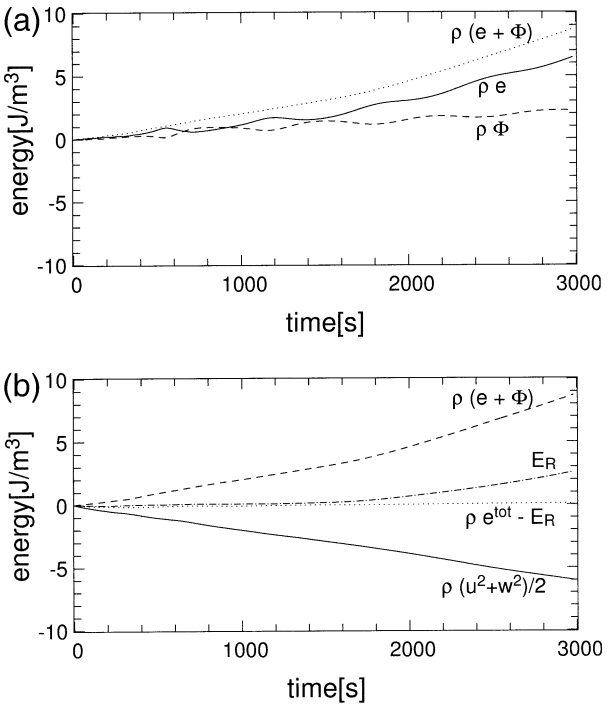

FIG. 7. The same as Figs. 3a and 3b but for the experiment of the finite amplitude topographic waves. In (b), energy change due to the damping terms E_R (dashed–dotted) and the difference between total energy ρe^{tot} and E_R (dotted) are added.

d. Topographic waves

Next, in order to examine the conservative property in the terrain following coordinate, we perform simulations of propagation of topographic waves induced by a surface topography in a uniform zonal wind field. The configuration of topography is given by

$$z_s = \frac{ha^2}{x^2 + a^2}. \tag{79}$$

Durran and Klemp (1983) give the maximum height $h = 1$ m to show an almost linear response. We also have calculated the same condition with $h = 1$ m and confirmed that our result is almost the same as Durran and Klemp (figures are not shown here). We also simulate the case with a finite amplitude $h = 1000$ m in order to examine how the energy is conserved. The horizontal length of the mountain is $a = 10$ km. The top of the model domain is $z_T = 16$ km, and the horizontal domain length is 180 km. The terrain-following coordinate ξ given by (48) is used. The grid intervals are $\Delta x = 2$ km and $\Delta\xi = 200$ m. Initially, temperature is constant 250 K, and the zonal wind is uniform $\bar{u} = 20$ m s^{-1}. In the layers above $\xi = 8$ km, we introduce damping terms that relax velocities and temperature to those of the basic initial fields. Similar to Durran and Klemp (1983), the relaxation rate of the damping has a cosine profile in the vertical. The damping time takes its shortest value $20\Delta t$ at the top of the model domain. The energy integration is based on the correction method. We will show results for a time step $\Delta t = 1$ s below. Note that we found that the time step can be extended as $\Delta t = 3$ s (the leapfrog time step is 6 s), which gives a sufficiently large Courant number for the vertical propagation of sound wave.

Figure 6 shows the structure of the perturbation of horizontal velocity u' and the vertical velocity w at $t = 3000$ s. The amplitudes of the velocities are about 1000 times larger than those of the analytic solution shown by Durran and Klemp (1983, their Figs. 1 and 2). At this time $t = 3000$ s ($\bar{u}t/a = 6$), the flow is not yet in the steady state. However, the further integration shows that turbulence develops due to the nonlinearity since this is the finite amplitude calculation; numerical diffusions are required to continue a stable calculation.

Figure 7 shows time sequences of energies. Since the damping terms are included above $\xi = 8$ km, the change in the total energy should be equal to the accumulation of the energy sinks due to the damping terms. In Fig. 7b, the accumulated energy change due to the damping terms is shown by the dashed–dotted curve E_R. It is found that E_R is almost explained by the damping term due to temperature perturbations (not shown). Figure 7b

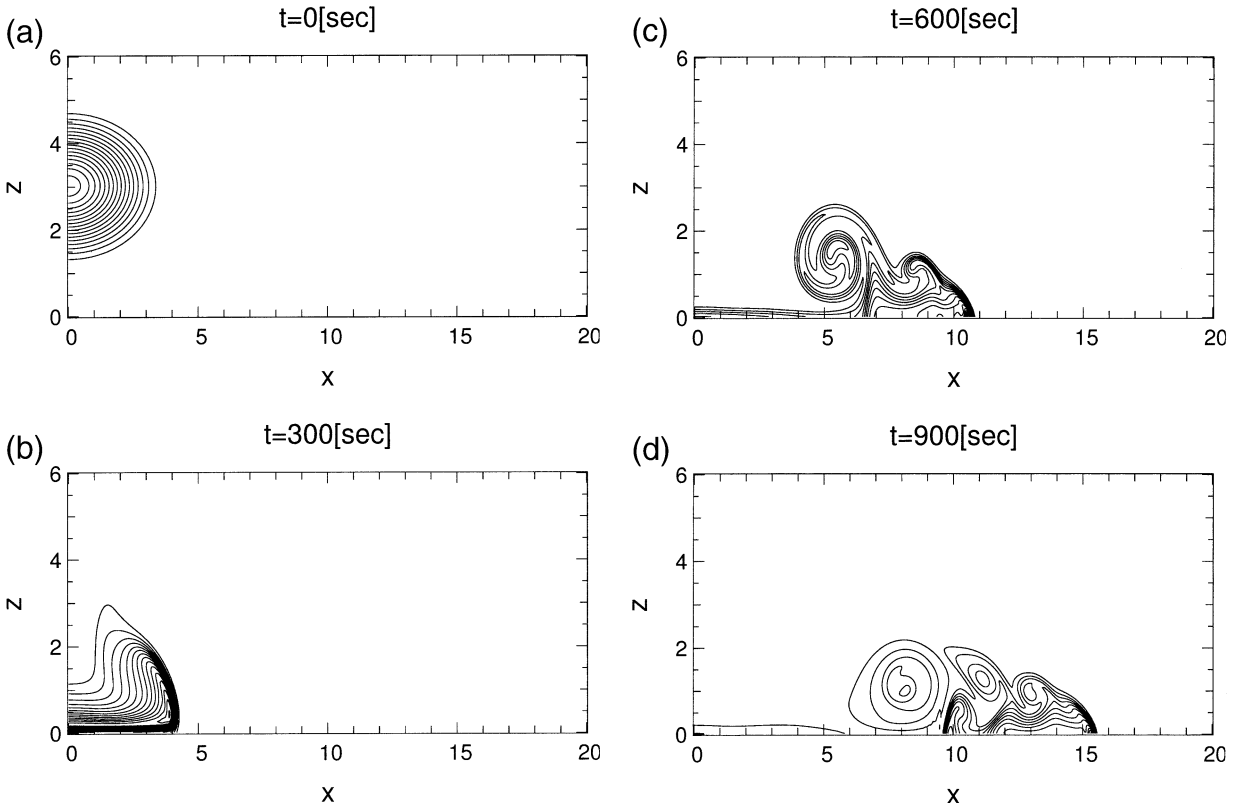

FIG. 8. Distributions of perturbations of potential temperature for the cold-bubble experiment with the grid interval $\Delta x = \Delta z = 50$ m at (a) the initial state, (b) $t = 300$, (c) 600, and (d) 900 s. The contour intervals are 1 K.

shows the difference between the change in the total energy and E_R by the dotted curve. It is confirmed that the change in the total energy is almost equal to E_R. Since this simulation is essentially linear, the energy conservation is well satisfied if the correction method is used. The mass is also almost conserved; the change in the mean density is about 10^{-14} kg m^{-3} for the 3000-s integration. This comes from the round-off errors.

e. Cold-bubble simulation

As a final example, we simulate the finite amplitude density current induced by a cold bubble given at the initial state. This experiment is suggested as a benchmark simulation of a nonlinear density current by Straka et al. (1993), and also used by Gallus and Rančić (1996). The basic thermal state is neutral and the initial perturbation of temperature, that is, a cold bubble, is given by

$$T' = \Delta T_0 \cos^2(\pi r^*/2), \tag{80}$$

$$r^* = \min\left\{1, \left[\left(\frac{x - x_m}{x_r}\right)^2 + \left(\frac{z - z_m}{z_r}\right)^2\right]^{1/2}\right\}, \tag{81}$$

where $\Delta T_0 = -15.0$ K, $x_r = 4.0$ km, $z_r = 2.0$ km, and $z_m = 3.0$ km. The domain size is 51.2 km in the horizontal, and 6.4 km in the vertical. We have tested the simulations for the grid intervals with $\Delta x = \Delta z = 50$, 100, and 200 m. The corresponding time step is $\Delta t = 0.05$, 0.1, and 0.2 s, respectively. The second-order diffusion is applied to the velocity and the temperature fields with the diffusion coefficient 75 m^2 s^{-1}. Note that the energy change due to the diffusion terms are almost negligible in this calculation.

The distributions of the perturbation of potential temperature at $t = 0$, 300, 600, and 900 s are shown in Fig. 8 for the 50-m grid simulation. The gravity current is propagating along the lower boundary and three rotors associated with the Kelvin–Helmholtz shear instability are well captured. The distribution of potential temperature at $t = 900$ s is comparable to the corresponding resolution experiment shown by Straka et al. (1993). Figure 9 compares the distributions of the perturbation of potential temperature at $t = 900$ s in the cases with the coarser resolutions 100 and 200 m. Since we only use the second-order centered-in-space scheme for the advection, the internal structure of vortices are not well simulated particularly in the case with the 200-m grid. However, as the resolution becomes finer, the representation of the rotors becomes better; this results indicate the confidence of the present scheme. The maximum and minimum values of perturbation of potential temperature at $t = 900$ s is 0.007000 K, -12.1084 K for

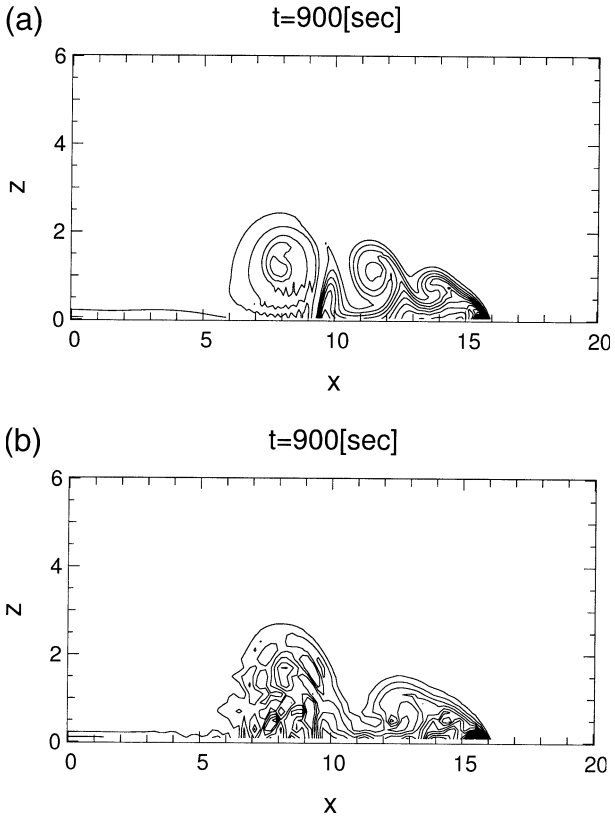

FIG. 9. The same as Fig. 8d but for the grid interval with (a) 100 and (b) 200 m.

the 50-m grid, 0.2178 K, −16.9435 K for the 100-m grid, and 2.2038 K, −21.6496 K for the 200-m grid. These values tend to converge to those of the reference solution presented by Straka et al. (1993).

Time sequences of energies for the simulation with the 50-m grid are displayed in Fig. 10. The nonlinear advective terms play important roles in this simulation. Strictly, the conservation of total energy is not satisfied in the correction scheme, if the advection of the kinetic energy is important. Reflecting this fact, the total energy is decreased by 5.12 J m^{-3} for the 900-s calculation as shown by Fig. 10b.

Gallus and Rančić (1996) developed a nonhydrostatic model with an energy conserving scheme using the pressure in the hydrostatic balance as a vertical coordinate. Gallus and Rančić (1996) have considered only the transformation term due to the pressure gradient force between the internal energy and the kinetic energy. Their scheme does not guarantee the exact conservation of total energy, hence it has the same limitation with the correction method. They also have shown the result of the cold-bubble experiment by using a grid interval of 100 m. In their calculation, their total energy is defined as the sum of the internal energy and the kinetic energy [Eq. (A.5) of Gallus and Rančić]. They stated that the change in the total energy is about 0.05% for the 40 000 iterations in the 900-s integration. In our

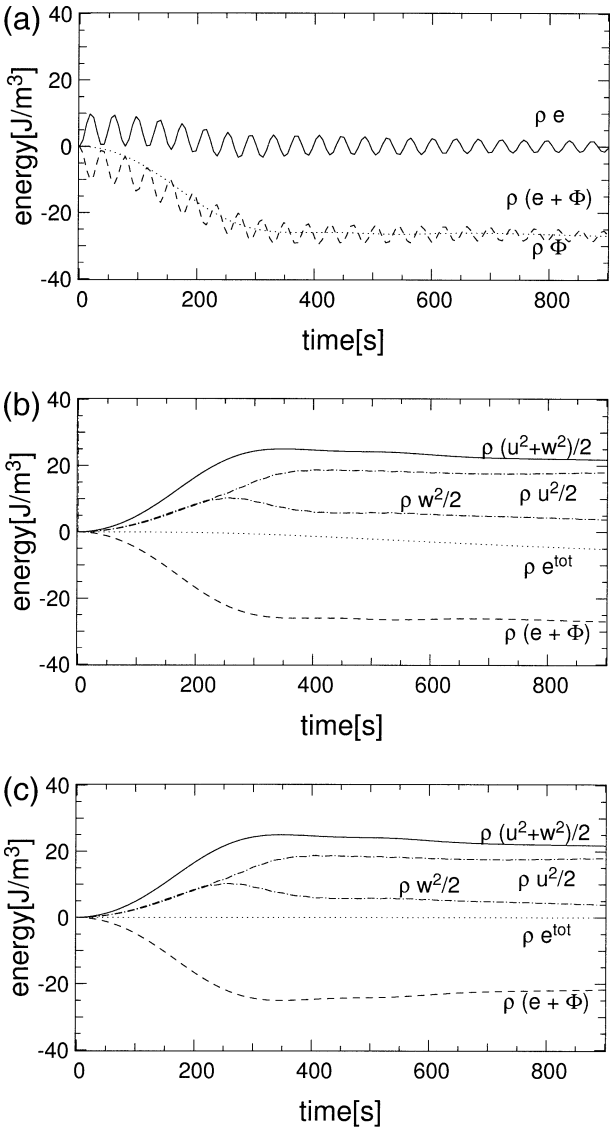

FIG. 10. The same as Figs. 3a and 3b but for the cold-bubble experiment. (a), (b) The correction method, and (c) the conservative method (see text).

calculation, since the initial value of the internal energy is 175 868 J m^{-3}, the corresponding change in the energy is 0.003% in the 18 000 steps integration. It may be said our result is superior to that of Gallus and Rančić in terms of the conservation of total energy.

As an alternative approach, we have performed the similar calculation of the cold-bubble experiment based on the conservative method. We found that the simulation is successfully performed without any instability. Figure 10c shows time sequences of energies, which are compared with Fig. 10b. The change in the total energy during 900 s is only −0.005 428 J m^{-3} for the 50-m grid, −0.010 84 J m^{-3} for the 100-m grid, and −0.025 28 J m^{-3} for the 200-m grid; the conservation is much

improved. This result suggests that the use of the conservation method is very encouraging.

5. Summary and discussions

We have devised a new dynamical scheme with the conservative forms of the nonhydrostatic models. It is aimed to apply to a global climate model for long time integrations in the future. In contrast to the past models based on the pressure and potential temperature as prognostic variables, the density and the internal energy are integrated in the flux forms. As a result, the conservation of total mass is satisfied within round-off errors. The conservation of total energy is approximately satisfied by considering the discretized forms of the major transformation terms of energy, though the exact conservation is not guaranteed since the inconsistency in the transformation of the nonlinear terms of the kinetic energy. We also argue about an alternative method in which the sum of internal energy and kinetic energy is used as a prognostic variable and the exact conservation of total energy is satisfied. We incorporated these schemes into a nonhydrostatic model with the horizontally explicit and vertically implicit time integration scheme for sound waves and performed various numerical experiments for the dry atmosphere. The numerical results show that the performance is comparative to that of the past studies, and that the proposed scheme is promising. In particular, the conservation of mass is confirmed with a great accuracy. The conservation of total energy is also demonstrated for the vertical propagation of sound waves, the horizontal propagation of gravity waves, and the finite amplitude topographic waves. The density current induced by an initial cold bubble is also calculated, which shows the approximate conservation of total energy. The propagation of the density current is successfully simulated if the sum of internal energy and kinetic energy is used as a prognostic variable. In this case, the conservation of total energy is much improved.

Recently, Klemp et al. (2000) take a similar approach to us by using the flux form equations for the conservation of variables. We summarize the differences between their scheme and ours. First, they have chosen density and potential temperature $\Theta = \rho\theta$ as prognostic variables; the choice of the density is similar to us but the use of the potential temperature may cause a problem in the climate modeling, as argued in section 3c. When Θ is integrated in the flux form, even if the domain integral of potential temperature is conserved, the change in the domain integral of total energy is not equal to the energy input from the boundaries, since temperature is diagnostically calculated. It may suffer from an artificial source other than the fluxes at the boundaries. By choosing Θ as a prognostic variable, the pressure gradient force term should be rewritten by using Θ. The pressure gradient is replaced by

$$\nabla p = \gamma R_d \pi \nabla \Theta. \tag{82}$$

If the right-hand side is discretized, a domain integral of momentum change is not equal to the difference between lateral boundary values of pressure; this implies that the conservation of momentum is incomplete, though the error might be small if this form is used only in the small step integration.

As another difference, they use ρw^* instead of $W = \rho w$ for the implicit calculation of the terrain following coordinate [Eq. (58)]. As shown by Eq. (58), the horizontal velocity components u and v are needed to calculate w^*. We solve for ρw but not for ρw^* in the implicit calculation; the vertical velocity is given by $w = J_x u + J_y v$ at the bottom boundary. In the integration of density, the convergence term associated with the vertical velocity is divided into two terms, one with $J_x u + J_y v$ and the other with w; this division might introduce relatively larger round-off errors. But the errors are small, and we think the choice of ρw is not a critical for the model performance.

When the time splitting method is introduced in the time integration, Klemp et al. (2000) propose that the advection term of energy should be split into the slow mode and the fast mode. They argue that the advection in the small time step is the deviation of the total advection from the advection related to the slow mode, and that sophisticated advection schemes such as semi-Lagrangian schemes should be incorporated into the discretization of the slow mode. Although we did not use any elaborated advection scheme and did not split the fast mode and the slow mode in the present simulations, introduction of the splitting of the advection term is worth considering for efficient calculations. We have done some preliminary tests of the time splitting for various experiments including horizontally propagating sound waves with basic winds. We have confirmed that the numerical calculation is stable even when the large time step is 10 times larger than the small time step.

In the present study, we only performed the simulations in the dry atmosphere. The properties of the conservations should be further examined in the case with the important hydrodynamic processes related to latent heat release. We will calculate the radiative–convective equilibrium in the two- or three-dimensional domains for the long time integrations such as several days (e.g., Held et al. 1993; Tompkins and Craig 1998b, 1999) and examine the conservations of the mass and the energy. We are planning to extend this dynamical model framework to the sphere and develop a global nonhydrostatic model for the climate modeling.

Acknowledgments. The author is grateful to Y. Kurihara, H. Tomita, M. Tsugawa, and T. Nasuno for helpful comments. The numerical calculations of the present study are done using HITACH SR8000 at the University of Tokyo under cooperative research with the Center for Climate System Research, University of Tokyo, NEC

SX4 at the National Institute of Environmental Studies, NEC SX5 at the Frontier Research System for Global Change, and the parallel computers at the High-Tech Research Center at Saitama Institute of Technology.

APPENDIX

Stability Analysis of the Implicit Scheme

In the scheme presented in section 2, the buoyancy term is also counted as an implicit term. This is for the consistency of the deformation of sound waves due to the stratification. In this appendix, we show the stability of the implicit scheme for sound and gravity waves in the isothermal atmosphere.

Before examination of the numerical scheme, we first derive the dispersion relations of sound waves and gravity waves in the horizontal–vertical two-dimensional isothermal atmosphere without diabatic and friction terms. The unperturbed state is in the hydrostatic balance (7) with the temperature T_s = constant. We start from the two-dimensional equations of (23), (24), (26), and (27) omitting the nonlinear terms and the heating and friction terms:

$$\frac{\partial}{\partial t}R + \frac{\partial}{\partial x}U + \frac{\partial}{\partial z}W = 0, \quad \text{(A1)}$$

$$\frac{\partial}{\partial t}U + \frac{\partial}{\partial x}P = 0, \quad \text{(A2)}$$

$$\frac{\partial}{\partial t}W + \frac{\partial}{\partial z}P + Rg = 0, \quad \text{(A3)}$$

$$\frac{\partial}{\partial t}P + c_s^2\frac{\partial}{\partial x}U + c_s^2\frac{\partial}{\partial z}W + \frac{R_d g}{C_v}W = 0, \quad \text{(A4)}$$

where we have used the relations $\partial E/\partial t = (C_v/R_d)\partial P/\partial t$ and $(R_d/C_v)h = c_s^2 = \gamma R_d T_s$ [see Eq. (36)]. Introducing the following variables

$$\hat{R} = \rho'/\sqrt{\rho_s} = R/\sqrt{\rho_s}, \qquad \hat{P} = p'/\sqrt{\rho_s} = P/\sqrt{\rho_s},$$
$$\hat{U} = \sqrt{\rho_s}u = U/\sqrt{\rho_s}, \qquad \hat{W} = \sqrt{\rho_s}w = W/\sqrt{\rho_s},$$

we rewrite Eqs. (A1)–(A4) as

$$\frac{\partial}{\partial t}\hat{R} + \left(\frac{\partial}{\partial z} - \frac{1}{2H}\right)\hat{W} = 0, \quad \text{(A5)}$$

$$\frac{\partial}{\partial t}\hat{U} + \frac{\partial}{\partial x}\hat{P} = 0, \quad \text{(A6)}$$

$$\frac{\partial}{\partial t}\hat{W} + \left(\frac{\partial}{\partial z} - \frac{1}{2H}\right)\hat{P} + \hat{R}g = 0, \quad \text{(A7)}$$

$$\frac{\partial}{\partial t}\hat{P} + c_s^2\left(\frac{\partial}{\partial z} - \frac{1}{2H}\right)\hat{W} + \frac{c_s^2 N^2}{g}\hat{W} = 0, \quad \text{(A8)}$$

where $H = -((1/\rho_s)\partial\rho_s/\partial z)^{-1} = R_d T_s/g$ and $N^2 = g^2/(C_p T_s)$ in the isothermal atmosphere. Assuming that $\hat{R}$, $\hat{P}$, $\hat{U}$, and $\hat{W}$ are proportional to $\exp[i(kx + mz - \omega t)]$, we have the dispersion relation:

$$\omega^4 - c_s^2(k^2 + m_H^2)\omega^2 + k^2 c_s^2 N^2 = 0, \quad \text{(A9)}$$

where $m_H^2 = m^2 + 1/(4H^2)$. In particular, the dispersion relations of sound waves and gravity waves are approximated given in the limit $N^2 \to 0$ and $c_s^2 \to \infty$: $\omega^2 = c_s^2(k^2 + m_H^2)$ and $\omega^2 = k^2N^2/(k^2 + m_H^2)$, respectively.

Next, we step to the stability analysis of the time discretized equations. The spatial structure is the same as the analytic forms: $(\hat{R}, \hat{U}, \hat{W}, \hat{P}) = (R, U, W, P)\exp[i(kx + mz)]$, and the discretization is introduced only in the time integration. We replace the time derivatives in Eqs. (A5)–(A8) by the discrete form δ_t, where $\delta_t A = (A^{n+1} - A^n)/\Delta t$ and introduce $\tilde{m} = m + i/2H$. We explicitly discretize the horizontal pressure gradient and implicitly discretize the other terms:

$$\delta_t R = -ikU^{n+1} - i\tilde{m}[\alpha W^{n+1} + (1 - \alpha)W^n], \quad \text{(A10)}$$

$$\delta_t U = -ikP^n, \quad \text{(A11)}$$

$$\delta_t W = -i\tilde{m}[\alpha P^{n+1} + (1 - \alpha)P^n] - g[\alpha R^{n+1} + (1 - \alpha)R^n], \quad \text{(A12)}$$

$$\delta_t P = -ikc_s^2 U^{n+1} - c_s^2(i\tilde{m} + N^2/g)[\alpha W^{n+1} + (1 - \alpha)W^n], \quad \text{(A13)}$$

where α is an implicit factor of the vertical propagation of sound wave. Here α represents the weight between the implicit and the explicit scheme: $\alpha = 0$ is for the explicit scheme, and $\alpha = 1$ is for the fully implicit scheme.

The above equations can be written as $AX^{n+1} = BX^n$, where $X = [R, U, W, P]^t$. The growth rate λ is the eigenvalue of the matrix $A^{-1}B$, and must satisfy $det(B - \lambda A) = 0$. From Eqs. (A10)–(A13), we have

$$\begin{aligned} 0 &= \det(B - \lambda A) \\ &= (1 - \lambda)^4 \\ &\quad + \Delta t^2 c_s^2\{k^2\lambda + m_H^2[(1 - \alpha) + \lambda\alpha]^2\}(1 - \lambda)^2 \\ &\quad + k^2\Delta t^4 c_s^2 N^2\lambda[(1 - \alpha) + \lambda\alpha]^2. \end{aligned} \quad \text{(A14)}$$

For the nearly vertically propagating sound waves with $k^2 \ll m_H^2$, the dispersion relation is approximated as

$$(1 - \lambda)^2 + \Delta t^2 c_s^2 m_H^2[(1 - \alpha) + \lambda\alpha]^2 = 0. \quad \text{(A15)}$$

From this, the growth rate is given by

$$|\lambda|^2 = \frac{1 + (1 - \alpha)^2\nu^2}{1 + \alpha^2\nu^2}, \quad \text{(A16)}$$

where $\nu^2 \equiv \Delta t^2 c_s^2 m_H^2$ is the Courant number. The scheme is stable $|\lambda|^2 \le 1$ irrespective of ν as long as $\alpha \ge \frac{1}{2}$. Figure A1 shows the dependency of $|\lambda|$ on ν. The dispersion relation (A9) and the growth rate (A16) become those of the simple sound waves without stratification as $H \to \infty$. Even when the buoyancy term is treated implicitly, therefore, the proposed numerical

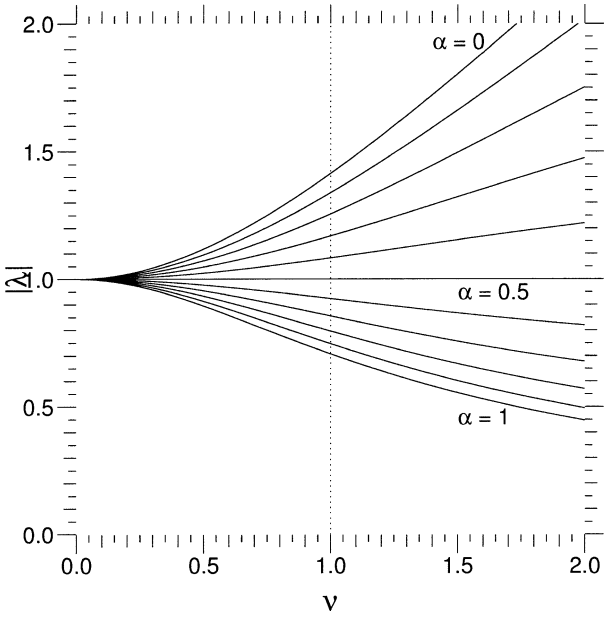

FIG. A1. Dependencies of the growth rate $|\lambda|$ on the Courant number ν and the implicit factor α.

scheme has the same stability condition as the usual implicit scheme for the sound waves.

For the quasi-horizontally propagating sound waves with $k^2 \gg m_H^2$ and $N^2 \approx 0$, the growth rate satisfies

$$(1 - \lambda)^2 + \Delta t^2 c_s^2 k^2 \lambda = 0. \quad \text{(A17)}$$

From this, the scheme is neutral $|\lambda| = 1$ if $\Delta t^2 c_s^2 k^2 \leq 1$ is satisfied.

The growth rate for gravity waves is approximately given in the limit $c_s \to \infty$ in Eq. (A14). In the case with $k^2 \gg m_H^2$, we have

$$(1 - \lambda)^2 + \Delta t^2 N^2 [(1 - \alpha) + \lambda\alpha]^2 = 0, \quad \text{(A18)}$$

from which the growth rate is

$$|\lambda|^2 = \frac{1 + (1 - \alpha)^2 \Delta t^2 N^2}{1 + \alpha^2 \Delta t^2 N^2}, \quad \text{(A19)}$$

Thus, the scheme is stable when $\alpha \geq \frac{1}{2}$. The dependency of the growth rate is the same as Fig. A1 but for $\nu = N\Delta t$. In the case with $k^2 \ll m_H^2$, on the other hand, we have

$$m_H^2(1 - \lambda)^2 + k^2 \Delta t^2 N^2 \lambda = 0. \quad \text{(A20)}$$

From this, the scheme is neutral $|\lambda| = 1$ as long as the time step satisfies $\Delta t^2 N^2 \leq m_H^2/k^2$, which is a less restrictive condition.

REFERENCES

Arakawa, A., and V. R. Lamb, 1977: Computational design of the basic dynamical processes of the UCLA general circulation model. *Methods Comput. Phys.,* **17,** 173–265.

——, and M. J. Suarez, 1983: Vertical differencing of the primitive equations in sigma coordinates. *Mon. Wea. Rev.*, **111,** 34–45.

Bonaventura, L., 2000: A semi-implicit semi-Lagrangian scheme using the height coordinate for a nonhydrostatic and fully elastic model of atmospheric flows. *J. Comput. Phys.,* **158,** 186–213.

Côté, J., S. Gravel, A. M'ethot, and A. Patoine, 1998a: The operational CMC–MRB global environmental multiscale (GEM) model. Part I: Design considerations and formulation. *Mon. Wea. Rev.,* **126,** 1373–1395.

——, J.-G. Desmarais, S. Gravel, A. Méthot, A. Patoine, M. Roch, and A. Staniforth, 1998b: The operational CMC–MRB global environmental multiscale (GEM) model. Part II: Results. *Mon. Wea. Rev.,* **126,** 1397–1418.

Cullen, M. J. P., T. Davies, M. H. Mawson, J. A. James, S. C. Coutler, and A. Malcolm, 1997: An overview of numerical methods for the next generation U.K. NWP and climate model. *Numerical Methods in Atmospheric and Oceanic Modelling, The Andrew J. Robert Memorial Volume*, C. A. Lin et al. Eds., NRC Research Press, 425–444.

Doms, G., and U. Schättler, 1997: The nonhydrostatic limited-are a model LM (Lokal–Modell) of DWD. Part I: Scientific Documentation. Deutscher Wetterdienst, 155 pp.

Durran, D. R., and J. Klemp, 1983: A compressible model for the simulation of moist mountain waves. *Mon. Wea. Rev.,* **111,** 2341–2361.

Gallus, W., Jr., and M. Rančić, 1996: A non-hydrostatic version of the NMC's regional Eta model. *Quart. J. Roy. Meteor. Soc.*, **122,** 495–513.

Held, I. M., R. S. Hemler, and V. Ramaswamy, 1993: Radiative–convective equilibrium with explicit two-dimensional moist convection. *J. Atmos. Sci.,* **50,** 3909–3927.

Juang, H.-M. H., 1992: A spectral fully compressible nonhydrostatic mesoscale model in hydrostatic sigma coordinates: Formulation and preliminary results. *Meteor. Atmos. Phys.,* **50,** 75–88.

Klemp, J. B., and R. B. Wilhemson, 1978: The simulation of three-dimensional convective storm dynamics. *J. Atmos. Sci.,* **35,** 1070–1096.

——, W. C. Skamarock, and J. Dudhia, cited 2000: Conservative split-explicit time integration methods for the compressible nonhydrostatic equations. [available online at http://wrf-model.org/WG1/wg1_main.html.]

Laprise, R., 1992: The Euler equations of motion with hydrostatic pressure as independent variable. *Mon. Wea. Rev.,* **120,** 197–207.

Morinishi, Y., T. S. Lund, O. V. Vasilyev, and P. Moin, 1998: Fully conservative higher order finite difference schemes for incompressible flow. *J. Comput. Phys.,* **143,** 90–124.

Ogura, Y., and A. Phillips, 1962: Scale analysis of deep and shallow convection in the atmosphere. *J. Atmos. Sci.,* **19,** 173–179.

Ooyama, K. V., 1990: A thermodynamic foundation for modeling the moist atmosphere. *J. Atmos. Sci.,* **47,** 2580–2593.

Qian, J.-H., F. H. M. Semazzi, and J. S. Scroggs, 1998: A global nonhydrostatic semi-Lagrangian atmospheric model with orography. *Mon. Wea. Rev.,* **126,** 747–771.

Semazzi, F. H. M., J. H. Qian, and J. S. Scroggs, 1995: A global nonhydrostatic semi-Lagrangian atmospheric model without orography. *Mon. Wea. Rev.,* **123,** 2534–2550.

Skamarock, W. C., and J. B. Klemp, 1992: The stability of time-split numerical methods for the hydrostatic and the nonhydrostatic elastic equations. *Mon. Wea. Rev.,* **120,** 2109–2127.

——, and ——, 1994: Efficiency and accuracy of the Klemp–Wilhemson time-splitting technique. *Mon. Wea. Rev.,* **122,** 2623–2630.

Smolarkiewicz, P. K., V. Grubisic, L. G. Margolin, and A. A. Wyszogrodzki, 1999: Forward-in-time differencing for fluids: Nonhydrostatic modeling of fluid motions on a sphere. *Proc. Seminar on Recent Developments in Numerical Methods for Atmospheric Modelling,* Reading, United Kingdom, ECMWF, 21–43.

Straka, J. M., R. B. Wilhemson, L. J. Wicker, J. R. Anderson, and K. K. Droegemeier, 1993: Numerical solutions of a nonlinear density current: A benchmark solution and comparisons. *Int. J. Numer. Methods Fluids,* **17,** 1–22.

Taylor, K. E., 1984: A vertical finite-difference scheme for hydrostatic and nonhydrostatic equations. *Mon. Wea. Rev.*, **112,** 1398–1402.

Tompkins, A. M., and G. C. Craig, 1998a: Time-scales of adjustment to radiative–convective equilibrium in the troposphere. *Quart. J. Roy. Meteor. Soc.*, **124,** 2693–2713.

——, and ——, 1998b: Radiative-convective equilibrium in a three-dimensional cloud ensemble model. *Quart. J. Roy. Meteor. Soc.*, **124,** 2073–2097.

——, and ——, 1999: Sensitivity of tropical convection to sea surface temperature in the absence of large-scale flow. *J. Climate*, **12,** 462–476.

Xue, M., K. K. Droegemeier, and V. Wong, 2000: The Advanced Regional Prediction System (ARP-S)—A multi-scale nonhydrostatic atmospheric simulation and prediction model. Part I: Model dynamics and verification. *Meteor. Atmos. Phys.*, **75,** 161–193.